Resonant light scattering by near-field-induced phonon polaritons

Jan Renger,* Stefan Grafström, and Lukas M. Eng
Institute of Applied Photophysics, University of Technology Dresden, D-01062 Dresden, Germany

Rainer Hillenbrand
Nano-Photonics Group, Max-Planck-Institut für Biochemie, D-82152 Martinsried, Germany
(Received 15 June 2004; published 18 February 2005; corrected 16 March 2005)

The scattering of light at a metallic nanoparticle in the vicinity of a SiC surface shows a strong peak around the surface phonon polariton resonance of the SiC substrate in the midinfrared spectral region. Close to the surface, the polarized particle couples to localized phonon polaritons. This near-field interaction shifts the peak to lower frequencies and causes a splitting into two modes for distances below 5 nm. We analyze this phenomenon by applying an accurate numerical three-dimensional model based on the multiple-multipole method. The results are compared with the predictions of the analytical dipole model as frequently used to explain the contrast in apertureless scattering-type scanning near-field optical microscopy. We find a qualitative agreement but the dipole model turns out to underestimate the spectral shift quantitatively.

DOI: 10.1103/PhysRevB.71.075410 PACS number(s): 07.79.Fc, 71.36.+c, 73.20.Mf, 68.37.Uv

I. INTRODUCTION

In the ongoing intense discussion on nano-optics, much attention is devoted to surface plasmon polaritons as a source of resonant field enhancement in the optical near field of metallic films and nanostructures.[1–3] Such resonances occur under the condition that the real part of the dielectric constant ϵ takes on an appropriate negative value. This is fulfilled in metals because of the free conduction electrons, and the resulting resonances of noble-metal nanoparticles mostly appear in the visible portion of the spectrum. It is much less known that surface plasmon polaritons have a counterpart in the infrared (IR) spectral region for some polar materials, caused by optical-phonon resonances. Here, $\mathrm{Re}(\epsilon)$ is negative in the so-called *reststrahlen* band between the transverse (TO) and longitudinal (LO) optical-phonon frequencies, which gives rise to the existence of so-called surface phonon polaritons (SPhPs). SPhPs offer attractive prospects for IR near-field optics. Their damping as characterized by $\mathrm{Im}(\epsilon)$ can be much weaker than for plasmons. The pronounced sharpness of the resonance opens the door to interesting applications in, for example, high-sensitivity sensorics, and various novel phonon-photonic devices have been conceived.[4] Furthermore, the influence of SPhPs on the near field of thermal emission was discussed in a theoretical paper.[5]

Recently, Hillenbrand *et al.* used a scattering scanning near-field optical microscope (s-SNOM) (Refs. 6–8) to study the scattering of infrared light at the metal-coated tip of a scanning force microscope in close proximity to a phonon-active SiC surface.[9] To single out the scattering caused by the near-field interaction between the tip and the sample, the distance was modulated and the resulting oscillation of the scattered field amplitude was demodulated at the second-harmonic frequency of the tip vibration. The observed signal exhibited a clear resonance at wave numbers around 930 cm^{-1}, indicating the excitation of a SPhP at the SiC surface via the near-field of the illuminated tip. The experiment provided evidence that IR spectroscopy with superb spatial resolution $<\lambda/100$ is possible.

The experimentally observed spectral response was in fair agreement with the simple dipole model of s-SNOM developed by Knoll and Keilmann.[10] This model describes the apex of the tip as a small polarizable sphere and uses electrostatics for calculating the modification of its dipole field caused by reflection at the sample surface. The model is appealing by its simple analytical treatment, but a number of approximations are expected to limit its validity. Due to the near-field interaction with the sample, the probe is expected to acquire higher multipole moments not taken into account in the dipole model. Furthermore, the quasi-electrostatic treatment neglects all retardation effects. Finally, the reduction of the tip to a sphere represents a very crude approximation to the true tip geometry.

In the present paper, we analyze the validity of the quasi-electrostatic dipole model by comparing its predictions with the results of a fully electrodynamic three-dimensional simulation. The calculations assume a Pt probe above a SiC surface, thereby mimicking the experimental arrangement of Ref. 9. After defining the parameters used in the calculations, we give a short survey of the basic ideas of the dipole model and apply it to the present case. Then, the numerical results are discussed in detail and compared with the simple dipole model in order to highlight its main deficiencies. At the end, we summarize the main findings and show that with some precautions the dipole model remains a very useful tool for the interpretation of s-SNOM data.

II. GEOMETRY, DIELECTRIC PROPERTIES, AND ILLUMINATION

We consider the arrangement depicted in Fig. 1. The probe is modeled as a Pt sphere or ellipsoid at a distance Δ from the surface of a SiC sample. The dielectric function of SiC in the interesting spectral region around 900 cm^{-1} is dominated by resonant phonon modes and may to a good

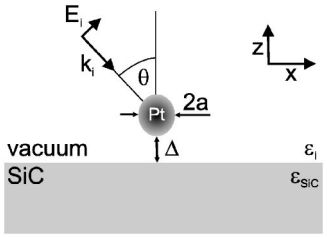

FIG. 1. Schematic of the model used for describing the near-field interaction between a metallic probe and a phonon-active sample.

approximation be described by a single Lorentzian-shaped resonance.[11]

$$\epsilon_{\mathrm{SiC}}(\nu) = 6.49 + \frac{3.23}{1 - \left(\frac{\nu}{\nu_0}\right)^2 - i\frac{\gamma\nu}{\nu_0^2}}, \tag{1}$$

with $\nu_0 = 788\ \mathrm{cm}^{-1}$ and $\gamma = 6.8\ \mathrm{cm}^{-1}$. As we focus our interest on how the sample rather than the probe influences the spectral response of the scattering, we assume a frequency-independent dielectric constant of the probe with a value applying to Pt around $900\ \mathrm{cm}^{-1}$: $\epsilon_{\mathrm{Pt}} = -1249 + 727i$.

Illumination is assumed to happen by a *p*-polarized plane wave incident at an angle θ. The superposition of the incident electric field $\mathbf{E_i}$ and the field $\mathbf{E_r}$ reflected off the sample surface constitutes the exciting field $\mathbf{E} = (E_x, E_y, E_z)$ to which the Pt particle is subjected. $\mathbf{E_i}$ and $\mathbf{E_r}$ are given by

$$\mathbf{E_i} = E_0 \begin{pmatrix} \cos\theta \\ 0 \\ \sin\theta \end{pmatrix} e^{i(k_x x + k_z z)} e^{-i\omega t}, \tag{2}$$

$$\mathbf{E_r} = r_{\parallel} E_0 \begin{pmatrix} -\cos\theta \\ 0 \\ \sin\theta \end{pmatrix} e^{i(k_x x - k_z z)} e^{-i\omega t}, \tag{3}$$

where E_0 is the incident amplitude, and $r_{\parallel}$ denotes the Fresnel reflection coefficient for *p* polarization:

$$r_{\parallel}(\epsilon_i, \epsilon_{\mathrm{SiC}}, \theta) = \frac{\epsilon_{\mathrm{SiC}} \cos\theta - \sqrt{\epsilon_i\, \epsilon_{\mathrm{SiC}} - \epsilon_i^2 \sin^2\theta}}{\epsilon_{\mathrm{SiC}} \cos\theta + \sqrt{\epsilon_i \epsilon_{\mathrm{SiC}} - \epsilon_i^2 \sin^2\theta}}, \tag{4}$$

with ϵ_i being the dielectric constant of the surrounding medium ($\epsilon_i = 1$ in the following). Figure 2 shows the electric-field components $|E_z|$ and $|E_x|$ above the interface as a function of incident angle θ and wave number ν. In the frequency region between $800\ \mathrm{cm}^{-1}$ and $900\ \mathrm{cm}^{-1}$ $\mathrm{Re}(\epsilon_{\mathrm{SiC}})$ is large and negative like in a metal and, hence, the electric field is essentially normal to the interface. For small incident angles θ, however, $|E_z|$ decreases due to the $\sin\theta$ term in $\mathbf{E_i}$. Conversely, around $\nu = 964\ \mathrm{cm}^{-1}$, where $\mathrm{Re}(\epsilon_{\mathrm{SiC}})$ passes through zero, the parallel component $|E_x|$ dominates (for $\epsilon_{\mathrm{SiC}} = 0$ the continuity of the normal component of the dielectric displacement at the interface requires $E_z = 0$). Figure 2 clearly shows that the dielectric response of the substrate gives rise to a strong frequency dependence of both the strength and ratio of the field components normal and parallel to the interface in the investigated frequency regime. In the following, we set θ to 45°.

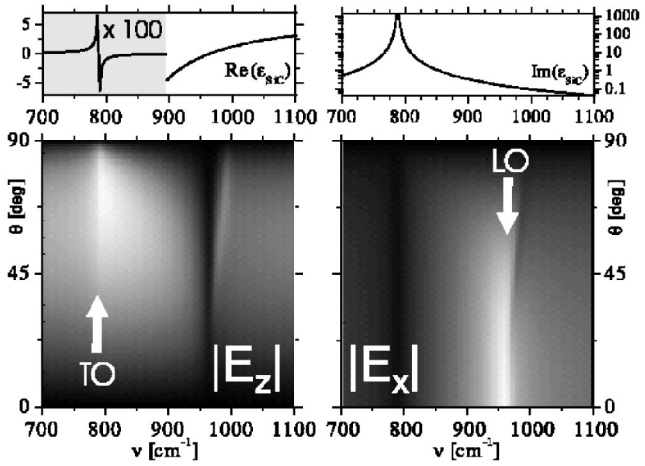

FIG. 2. The temporally averaged electric field components $|E_z|$ normal and $|E_x|$ parallel to the SiC interface plotted as a function of incident angle θ and wave number ν. The gray scale ranges from 0 (black) to $1.5 \times |E_0|$ (bright). The upper graphs display the dielectric function of SiC. The pronounced variation of $\epsilon_{\mathrm{SiC}}(\nu)$ is caused by a phonon resonance. $\mathrm{Re}(\epsilon)$ is negative in the *reststrahlen* band between the transverse and longitudinal optical-phonon frequencies indicated by TO and LO, respectively. This leads to the clear spectral dependence of $|E_z|$ and $|E_x|$ as seen in the gray scale maps.

III. THE QUASI-ELECTROSTATIC DIPOLE MODEL

The quasi-electrostatic theory[12] is one of the simplest approaches to describing the tip-sample interaction and has successfully been used to explain the image contrast in near-field optical microscopy.[9,10] Applicability of this static theory to the scattering problem is limited to the case that the size of the particle and its distance to the sample surface are much smaller than the wavelength λ, so that retardation can be neglected (Rayleigh limit). In the present case of midinfrared radiation ($\lambda \approx 10.6\ \mu\mathrm{m}$) this condition is indeed much better fulfilled than in the visible regime.

The dipole model describes the probe as a sphere with radius *a* that becomes polarized by the local field according to its polarizability α:

$$\alpha = 4\pi a^3 \frac{\epsilon_{\mathrm{Pt}} - \epsilon_i}{\epsilon_{\mathrm{Pt}} + 2\epsilon_i}. \tag{5}$$

In the vicinity of an interface, the dipole field generated by the sphere is reflected and reinteracts with the sphere. In the quasi-electrostatic approach, the coupled system can be described by the superposition of the sphere's original field and the field from an image dipole in the substrate. This changes the local field at the position of the sphere, thereby modifying its dipole moment. The total field radiated to the far field can be attributed to the total dipole moment made up of the sphere and its image charge distribution. The result can conveniently be written in terms of an effective polarizability α_{eff} connecting the total dipole moment of the probe-sample

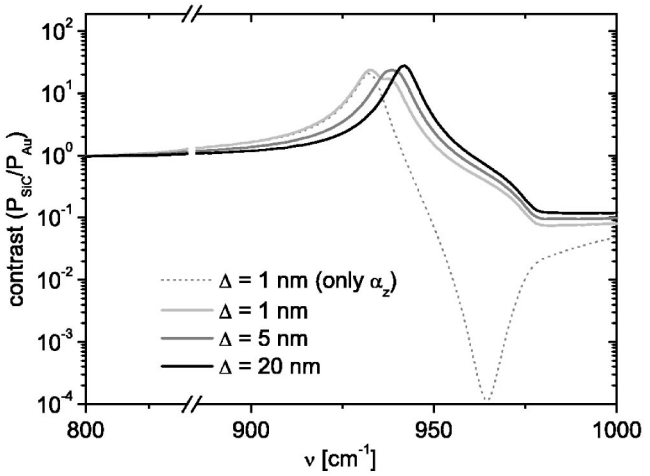

FIG. 3. Power scattered by a spherical Pt probe above a SiC surface, normalized to the power obtained for a Au substrate. For large separation ($\Delta=20$ nm) scattering is strongest around 942 cm^{-1} corresponding to $\mathrm{Re}(\epsilon_{\mathrm{SiC}})\approx -1$. When the probe is moved toward the sample, this maximum broadens and shifts to 939 cm^{-1} ($\Delta=5$ nm), and finally splits into two peaks at 933 cm^{-1} and 938 cm^{-1} ($\Delta=1$ nm). The dotted curve was calculated for a purely vertical exciting field and exhibits a single maximum at 933 cm^{-1}.

system to the exciting field **E**. The effective polarizability α_{eff} has the following tensor elements normal and parallel to the interface:

$$\alpha_{\mathrm{eff},z}=\frac{\alpha(1+\beta)}{1-\frac{\alpha\beta}{16\pi h^3}},\quad \alpha_{\mathrm{eff},x}=\frac{\alpha(1-\beta)}{1-\frac{\alpha\beta}{32\pi h^3}}, \tag{6}$$

where $h=\Delta+a$ indicates the distance between the point dipole at the center of the Pt sphere and the SiC interface (see Fig. 1). The latter is characterized by its surface response function $\beta=(\epsilon_{\mathrm{SiC}}-1)/(\epsilon_{\mathrm{SiC}}+1)$, which has a pole for $\epsilon_{\mathrm{SiC}}=-1$. The total scattered power P_{tot} is proportional to the square modulus of the total dipole moment times the fourth power of the frequency:

$$P_{\mathrm{tot}}\propto \nu^4\{|\alpha_{\mathrm{eff},x}E_x|^2+|\alpha_{\mathrm{eff},z}E_z|^2\}. \tag{7}$$

To facilitate an easy comparison with experiments, the power P_{SiC} scattered by the Pt probe above the SiC substrate is normalized to the power P_{Au} scattered when SiC is replaced by gold with $\epsilon_{\mathrm{Au}}=-5000+1000i$. This material contrast V defined as

$$V=\frac{P_{\mathrm{SiC}}}{P_{\mathrm{Au}}} \tag{8}$$

can easily be determined and is not distorted by the ν^4 dependence of the total scattered power.

Figure 3 displays the spectral dependence of V as obtained from the quasi-electrostatic theory for a Pt sphere with radius $a=20$ nm. At large separation $\Delta=20$ nm, the curve is dominated by the pole of β, which leads to a maximum of the effective polarizability close to 942 cm^{-1}, where $\mathrm{Re}(\epsilon_{\mathrm{SiC}})\approx -1$. At smaller distances, the near-field interaction between probe and sample, as represented by the denominators of $\alpha_{\mathrm{eff},z}$ and $\alpha_{\mathrm{eff},x}$ in Eq. (6), becomes more important. Consequently, the maximum shifts differently for the two field components parallel and normal to the interface. As a result, the maximum broadens and shifts to 939 cm^{-1} for $\Delta=5$ nm. Finally, close to contact at $\Delta=1$ nm, the peak splits into two separate modes. The different origin of the two maxima becomes clear when E_x is set to zero in the calculation of V. Then, only the more pronounced maximum at 933 cm^{-1} remains (see dotted curve in Fig. 3). Hence, this resonance, which is shifted to a frequency for which $\mathrm{Re}(\epsilon_{\mathrm{SiC}})\approx -1.5$, is excited by the normal field component, whereas the less shifted peak at 938 cm^{-1} originates from the parallel component. Around 964 cm^{-1}, suppression of E_x leads to a deep minimum of V, caused by an almost complete vanishing of E_z in this frequency range (see Fig. 2). In the following, we refer to the two modes as the normal and the parallel mode, respectively.

IV. NUMERICAL RESULTS

The electrostatic theory discussed above describes the probe-sample interaction as an instantaneous process, neglecting all effects due to retardation, and furthermore makes the basic assumption that the scatterer may be described as a simple point dipole at the center of the sphere. To check the validity of such a description we used the multiple-multipole (MMP) technique[13] for solving Maxwell's equations and satisfying the boundary conditions. This versatile semianalytical boundary method expresses the electric and magnetic fields as a superposition of known exact solutions of Maxwell's equations, such as plane waves, multipole fields, or waveguide modes. By minimizing the error at the boundary, the code computes the expansion coefficients that best satisfy the boundary conditions. MMP's big advantage is that only the boundary needs to be discretized. With the use of appropriate basis functions, the numerical effort remains reasonably small and the solution can be very accurate. The average relative mismatch at the boundary typically stays far below 0.1% for all results presented in this paper.

A. Scattering signature of a sphere

Again, we start our discussion by considering the situation for a fairly large separation $\Delta=20$ nm between the spherical Pt scatterer and the SiC surface. Figure 4 displays the electric-field distribution $|E|$ surrounding the sphere for various frequencies ν. Around 800 cm^{-1}, the SiC substrate behaves metal-like. Therefore, the electric field above the sample is dominated by the normal component (see Fig. 2) resulting in a polarization of the sphere along the z axis. For higher ν (less metallic behavior), this situation changes. Near 910 cm^{-1}, $|E_z|$ and $|E_x|$ are comparable in size and phase shifted by $\approx\pi/2$ with respect to each other, so that they produce an almost circularly polarized electric field leading to a rotating dipole in the sphere. Therefore, $|E|$ is almost uniform along the circumference of the sphere in the xz plane. Around 940 cm^{-1} [$\mathrm{Re}(\epsilon_{\mathrm{SiC}})\approx -1$] excitation of SPhPs

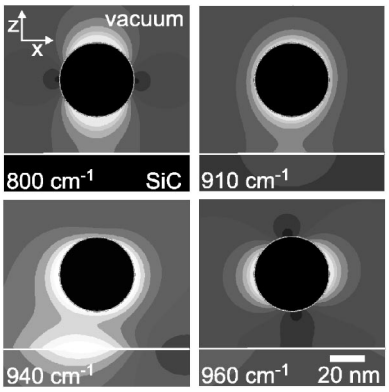

FIG. 4. Electric-field amplitude $|E|$ around a Pt sphere 20 nm above a SiC surface at four different frequencies. The spectral dependence of the sphere polarization mainly follows the frequency dependence of the exciting field (see Fig. 2). The metal-like behavior of the substrate at 800 cm^{-1} results in a polarization normal to the interface. The parallel component dominates at higher frequencies. Around 940 cm^{-1} [$\mathrm{Re}(\epsilon_{\mathrm{SiC}}) \approx -1$] localized surface waves are excited. Bright colors correspond to high $|E|$.

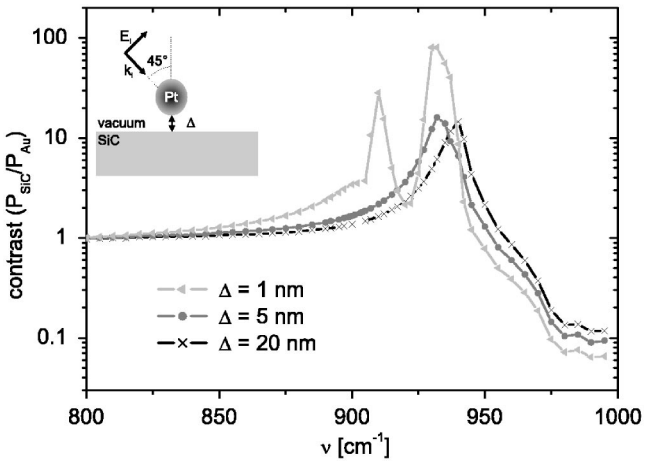

FIG. 5. Power scattered by a spherical Pt probe above SiC normalized to the power obtained with a Au substrate. For large $\Delta = 20$ nm, the scattering is resonantly enhanced near 940 cm^{-1} corresponding to $\mathrm{Re}(\epsilon_{\mathrm{SiC}}) \approx -1.1$. At smaller distances, this maximum shifts to 932 cm^{-1} for $\Delta = 5$ nm, and additionally splits into two peaks at 910 cm^{-1} and 932 cm^{-1} for $\Delta = 1$ nm.

becomes resonant. For large k values in the surface plane, the SPhP dispersion relation asymptotically approaches the frequency for which $\mathrm{Re}(\epsilon_{\mathrm{SiC}}) = -1$. Therefore, close to this frequency a localized SPhP wave packet made up of essentially standing waves with short wavelengths can be excited. The necessary large k vectors are provided by the near field of the polarized sphere. Due to momentum conservation, this process is forbidden if the scatterer is absent. This excitation leads to a pronounced field distortion with a strong field near the sample surface. Beyond this surface resonance, at 960 cm^{-1}, the sphere becomes polarized along the x axis, in accordance with the electric field being essentially parallel to the interface as illustrated in Fig. 2.

In summary, the interaction between the sphere and the SiC substrate is rather weak if they are separated by some ten nanometers. The probe polarization is more or less directly determined by the exciting field above the sample. This picture changes only when excitation of SPhPs becomes possible, which leads to an appreciable probe-sample interaction. Such near-field properties are important for all processes that are sensitive to the local electric field, such as Raman scattering and surface-enhanced infrared absorption (SEIRA).[14] In the context of surface-enhanced spectroscopy, the excitation of the surface polariton via a conducting sphere was also considered in an earlier work by Aravind and Metiu, who introduced the name "gap mode" for the resulting resonance of the coupled system.[15]

To compare our numerical findings with the dipole model, we again calculate the normalized ratio V, which reflects the signature to be expected in a s-SNOM experiment where the radiated power is detected in the far field. Figure 5 depicts the spectral dependence of V as derived from the numerically calculated far-field distribution for different separations Δ. This plot may be directly compared with the results of the dipole model displayed in Fig. 3. Due to excitation of surface waves and their scattering by the sphere, the spectrum exhibits a maximum around 940 cm^{-1} for $\Delta = 20$ nm. Moving the scatterer closer to the interface shifts this resonance to 932 cm^{-1} for $\Delta = 5$ nm. At an even smaller distance of $\Delta = 1$ nm, the maximum splits into two clearly separated peaks at 910 cm^{-1} and 932 cm^{-1}.

There is a satisfactory overall agreement between the results of the accurate numerical model and the predictions of the quasi-electrostatic dipole model. The latter reproduces the SPhP resonance in a qualitatively correct way. However, there are clear quantitative discrepancies for small probe-sample separations in the spectral region of the resonance. For $\Delta = 1$ nm, the splitting and shift of the two modes as well as their enhancement are much less pronounced in the dipole model (splitting $\Delta\nu \approx 5$ cm^{-1}, see Fig. 3) than in the MMP results ($\Delta\nu \approx 22$ cm^{-1}, Fig. 5). Furthermore, V is three times smaller at 910 cm^{-1} than at 932 cm^{-1} according to the numerical treatment, whereas the dipole model predicts the lower-frequency normal mode to be the stronger one.

Inspection of the electric-field distribution at the maxima provides some insight into the nature of the two resonant modes (Fig. 6). As seen in the snapshots depicted in the lower part of the figure, the electric field directly underneath the probe points predominantly along the z direction in case of the normal mode (910 cm^{-1}), in accordance with the vertically oriented dipole moment of the sphere. The parallel mode, on the other hand, shows a more complicated field pattern. To accommodate the horizontal dipole moment of the sphere, the field has to reverse its direction over a very short distance along the x axis. This corresponds to excitation of surface waves with very high k vectors, which explains why this mode is higher in frequency (932 cm^{-1}).

To conclude this section, we note that reduction of the scattering sphere to a simple point dipole at the sphere's center, as assumed by the dipole model, turns out to be a rather crude approximation for small separations, especially close to the substrate-induced resonance. Just above the in-

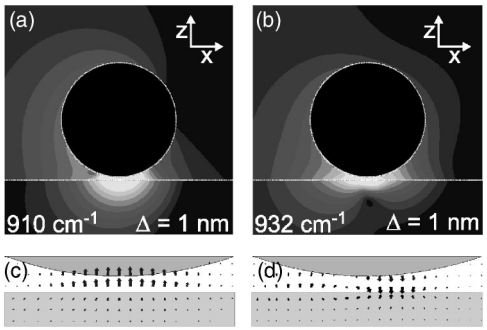

FIG. 6. (a) and (b) Electric-field amplitude $|E|$ around a Pt sphere 1 nm above the interface. The data are displayed on a logarithmic gray scale with successive hues differing by a factor of 2. The electric-field patterns in (c) and (d) (reflecting one specific moment in time) reveal the different field directions for the two resonances. At 910 cm^{-1}, the field underneath the tip is more or less uniformly oriented along the z direction, whereas at 932 cm^{-1} the field reverses its direction from $-z$ to $+z$ across a short distance along the x axis.

terface, the electric field generated by the image charge results in a strongly inhomogeneous field across the sphere, which produces a charge distribution that cannot be described as a pure dipole. However, the validity of the dipole approximation can in fact be restored to some extent if the position of the dipole is shifted from the center of the sphere toward the interface. This effective displacement becomes increasingly pronounced with decreasing separation Δ between sphere and interface. For example, at $\Delta=1$ nm, a shift of the dipole by 4.3 nm makes the resonances predicted by the analytical model coincide within ~ 1 cm^{-1} with those found numerically. However, the amplitude ratio of the two peaks is still not reproduced correctly. This confirms that also higher-order multipoles have to be taken into account in a refined model, as pointed out by Porto *et al.*[16]

B. Scattering signature of an ellipsoid

Modeling the s-SNOM probe by a sphere represents the simplest approach only and may be too far from the real experiment in which probing is realized by scattering the near field at a sharp metallic tip.[6–8] Such a probe is highly anisotropic with respect to its polarizability parallel and normal to the sample surface. To investigate the influence of the probe geometry on the spectral response, we replaced the sphere by a prolate Pt ellipsoid having a length and width of 100 nm and 30 nm, respectively.

The larger volume of the ellipsoid results in a larger scattered power in absolute numbers, but again we prefer to consider the relative contrast V versus a gold sample [see Fig. 7(a)]. If the ellipsoid and the substrate are separated by $\Delta=20$ nm, the resonance is centered around 937 cm^{-1}. Getting closer to $\Delta=5$ nm shifts the resonance toward 935 cm^{-1}, while for $\Delta=1$ nm the modes appear separated at 917 cm^{-1} and 935 cm^{-1}. Because of the higher polarizability along the long axis,[17] the resonance peak at 917 cm^{-1} (normal mode) is now the more pronounced one with an amplitude twice as high as the maximum at 935 cm^{-1} (parallel

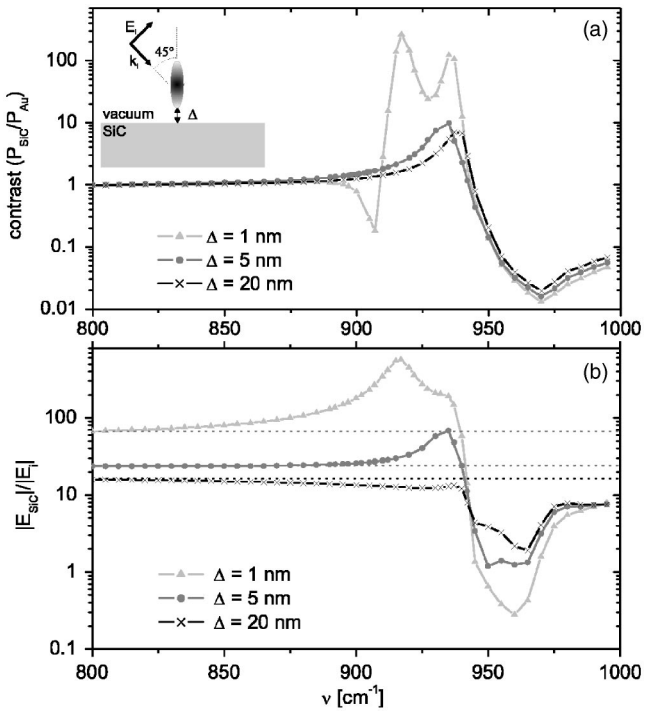

FIG. 7. (a) Scattered power for a 100 nm long and 30 nm wide ellipsoidal Pt probe above SiC, normalized to a Au substrate. The spectra show a similar splitting of the resonance for small separations like in the case of a spherical probe (Fig. 5), however with a slightly smaller shift of the maxima to 917 cm^{-1} and 935 cm^{-1} for $\Delta=1$ nm, and to 935 cm^{-1} for $\Delta=5$ nm. (b) Electric-field enhancement at the lower end of the ellipsoidal probe above a resonant SiC substrate (solid curves) compared with the behavior of the same particle above a nonresonant Au substrate (dotted lines).

mode). The normal mode is significantly less frequency shifted than for a spherical probe. This can be attributed to a larger effective distance between the sample and the probe dipole for the elongated ellipsoid as compared to the sphere. In the frequency range above the resonance, where E_z becomes small and the field is dominated by E_x (see. Fig. 2), the smaller polarizability along the short axis leads to a minimum of V, which was not present in the previously considered case of a sphere unless E_x was artificially set to zero (see Fig. 3).

In summary, the shape of the probe has a clear influence on the spectral dependence of the scattering. However, as the resonance originates from the sample, this influence is not as dramatic as it would be if the resonance had its origin in the polarizability of the probe. In this latter case of a particle polariton, frequently considered in the literature as a means of enhancing the scattering, the probe geometry is one of the key parameters determining the resonant frequency. In real experiments, the shape of the probe is often rather ill defined, which makes it difficult to fulfill the resonance condition of such a probe polariton in a reproducible way. A resonance residing in the sample, as treated in the present paper, offers the advantage of being much more robust versus variations of the geometry and material composition of the probe.

Finally, we turn our attention to the enhancement of the electric-field strength at the very end of the ellipsoid, repre-

senting the tip apex. Figure 7(b) displays the field enhancement $|E_{\mathrm{SiC}}|/|E_0|$ with respect to the incident field. If, for comparison, the SiC sample is replaced by Au, the field enhancement takes on the values indicated by dotted lines. For the latter system, consisting of two nonresonant materials (Au substrate and Pt probe), $|E|$ increases by a factor of 1.5 when the distance Δ is reduced from 20 nm to 5 nm, and by another factor of 2.8 upon further reduction of Δ to 1 nm. The resonance produced by the SiC surface leads to an enhancement that is higher by as much as a factor of 8.4 for the smallest separation. This increased electric field very close to the interface may be used to gain sensitivity and lateral resolution, e.g., in SEIRA measurements. For larger separations, the factor in favor of SiC drops to 2.9 at $\Delta = 5$ nm and to <1 at $\Delta = 20$ nm. The reason for this behavior is that at larger distances Δ, the favorable influence of the surface resonance in SiC becomes weaker. Under these circumstances, the resulting field turns out to be stronger for a gold sample simply because of the higher reflectivity of the metal surface.

V. DISCUSSION AND SUMMARY

We have performed a detailed comparison between a simple analytical model used to describe s-SNOM and the results of a numerical analysis of the full electrodynamic problem. The MMP method was used to analyze the interaction of light in the midinfrared spectral region with a small metal particle above a planar SiC surface. In this material, excitation of surface phonon polaritons leads to strong resonances in the scattering signature. The presence of the sphere cancels the requirement of momentum conservation and, hence, localized surface wave excitation becomes possible. For a separation between the particle and the interface of some ten nanometers, the resonance is centered around the frequency where $\mathrm{Re}(\epsilon_{\mathrm{SiC}}) \approx -1$. For smaller separations, the near-field interaction arising from the stronger coupling between the polarized sphere and the SPhPs causes a shift toward more negative ϵ values. Finally, below a distance of 5 nm, the resonance splits into two modes coupling to different field components. This behavior is reproduced qualitatively also by the quasi-electrostatic dipole model which, however, underestimates both the spectral shift and splitting, and also provides the wrong intensity ratio of the two modes. Off resonance, the quasi-electrostatic and the numerical model produce nearly identical results.

The main weakness of the analytical model is not the electrostatic approximation, which actually is well fulfilled in the wavelength regime under consideration. It is rather the replacement of the scatterer by a point dipole at its center that becomes invalid at small distances. Then, the dipole is effectively displaced from the center of the probe and, additionally, higher-order multipoles begin to play a role. In fact, the experimental data in Refs. 9 and 19 confirm that the shift is stronger than predicted by the dipole model. With an effective reduction of the distance of the probe dipole from the surface, the stronger shift of the resonance can, however, still essentially be understood within the dipole model. The pronounced dependence of the resonant frequency on the distance at small separations has a clear impact on experiments in which the distance is modulated. To take the most advantage of the SPhP resonance and to achieve the highest spatial resolution, one should choose the wavelength such that it fits the resonance at the inner turning point of the probe vibration.

Furthermore, the analytical model treats the probe as a sphere, far from the real shape of s-SNOM probes. Our MMP results obtained for an ellipsoidal scatterer show that variation of the probe geometry leaves the coarse signature of the resonance unchanged but has a clear influence on the details of the spectral response. In particular, a vertically elongated probe tends to favor the resonant mode related to the normal field component. Note that by considering the contrast versus a gold sample, we suppress the overall ν^4 frequency dependence of the scattered power, thereby emphasizing the spectral features arising from the tip-sample interaction. Therefore, we expect the main trends to remain valid also for probes with a more realistic conical shape, even though such a geometry leads to a much weaker overall frequency dependence.[18]

Recently, similar resonance shifts were observed experimentally by s-SNOM probing of SiC.[19] However, only one resonance was observed.[9,19] This might indicate that the antenna properties of a real cone-shaped probe lead to an even stronger enhancement of the normal mode as compared to a prolate spheroid. However, additional effects may contribute to the observed behavior. Namely, in the experiment, the s-SNOM probe was vibrated along the surface normal with an amplitude of some tens of nanometers, which makes the SPhP resonances oscillate in spectral position, thereby blurring them. Furthermore, in Ref. 19, the SiC sample was highly doped and therefore exhibited larger damping. An analysis within the dipole model shows that such an increase of $\mathrm{Im}(\epsilon)$ affects the parallel mode more strongly than the normal one. A definitive answer to the question as to which role the parallel mode plays in the case of conical probes and under what conditions it may become visible in the experiment requires a numerical treatment of the conical geometry.

In conclusion, our complete numerical analysis shows the limitations of the dipole model. However, with the general trends revealed by the MMP results in mind, one has a guideline at hand for exploiting in a more reliable way the big advantage of the dipole model of being an analytical tool for the analysis of s-SNOM data.

ACKNOWLEDGMENTS

This research was supported by the Deutsche Forschungsgemeinschaft (Graduiertenkolleg Sensorik). The authors thank the Zentrum für Hochleistungsrechnen of the University of Technology Dresden for providing computational resources. One of the authors (R. H.) thanks the Bundesministerium für Bildung und Forschung (BMBF) for financial support (Nachwuchswettbewerb Nanotechnologie 2002).

*Author to whom correspondence should be addressed; electronic mail: renger@iapp.de

[1] H. Raether, *Surface Plasmons* (Springer, Berlin, 1988).
[2] M. Quinten, A. Leitner, J. Krenn, and F. Aussenegg, Opt. Lett. **23**, 1331 (1998).
[3] J. Renger, S. Grafström, V. Deckert, and L. M. Eng, J. Opt. Soc. Am. A **21**, 1362 (2004).
[4] R. Hillenbrand, Ultramicroscopy **100**, 421 (2004).
[5] A. V. Shchegrov, K. Joulain, R. Carminati, and J.-J. Greffet, Phys. Rev. Lett. **85**, 1548 (2000).
[6] Y. Inouye and S. Kawata, Opt. Lett. **19**, 159 (1994).
[7] M. Specht, J. D. Pedarnig, W. M. Heckl, and T. W. Hänsch, Phys. Rev. Lett. **68**, 476 (1992).
[8] R. Bachelot, P. Gleyzes, and A. C. Boccara, Microsc. Microanal. Microstruct. **5**, 389 (1994).
[9] R. Hillenbrand, T. Taubner, and F. Keilmann, Nature (London) **418**, 159 (2002).
[10] B. Knoll and F. Keilmann, Opt. Commun. **182**, 321 (2000).
[11] F. Engelbrecht and R. Helbig, Phys. Rev. B **48**, 15 698 (1993).
[12] J. D. Jackson, *Klassische Elektrodynamik*, 2nd ed. (de Gruyter, Berlin, 1982).
[13] C. Hafner, *The Generalized Multipole Technique for Computational Electromagnetics* (Artech House, Boston, 1990).
[14] M. S. Anderson, Appl. Phys. Lett. **83**, 2964 (2003).
[15] P. K. Aravind and H. Metiu, J. Phys. Chem. **86**, 5076 (1982).
[16] J. A. Porto, P. Johansson, S. P. Apell, and T. López-Ríos, Phys. Rev. B **67**, 085409 (2003).
[17] C. F. Bohren and D. R. Huffman, *Absorption and Scattering of Light by Small Particles* (Wiley, New York, 1983).
[18] L. Aigouy, F. X. Andréani, A. C. Boccara, J. C. Rivoal, J. A. Porto, R. Carminati, J.-J. Greffet, and R. Mégy, Appl. Phys. Lett. **76**, 397 (2000).
[19] T. Taubner, F. Keilmann, and R. Hillenbrand, Nano Lett. **4**, 1669 (2004).